Article:
Vakurov, A, Mokry, G, Drummond-Brydson, R et al. (3 more authors) (2013) ZnO nanoparticle interactions with phospholipid monolayers. Journal of Colloid and Interface Science, 404. 161 - 168. ISSN 0021-9797

https://doi.org/10.1016/j.jcis.2013.05.010

ZnO nanoparticle interactions with phospholipid monolayers

Alex Vakurov[a], Guillermo Mokry Lopez[a], Rik Drummond-Brydson[b], Rachel Wallace[b], Claus Svendsen[c] and Andrew Nelson[a]

Schools of [a]Chemistry and [b]Process, Environmental and Materials Engineering, University of Leeds, Leeds, LS2 9JT, UK.

[c]NERC Centre for Ecology and Hydrology, Wallingford, UK

Authors' e mail addresses: A.V.Vakourov@leeds.ac.uk, guillermo.mokry@gmail.com, R.M.Drummond-Brydson@leeds.ac.uk, r.wallace06@leeds.ac.uk, csv@ceh.ac.uk

Corresponding author:

Professor Andrew Nelson

Phone: +44 (0)113 343 6409

Fax: +44 (0)113 343

Email: a.l.nelson@leeds.ac.uk

Abstract

Aqueous ZnO nanoparticle dispersions interaction with a dioleoyl phosphatidylcholine (DOPC) monolayer is reported in this paper. ZnO-DOPC interactions were investigated using rapid cyclic voltammetry (RCV) by focusing on the effect of the interactions on the characteristics of the capacitance current peaks representing two potential induced phase transitions. Results showed:- (1) The order of interaction of common commercially sourced nanoparticles with DOPC coated Hg electrodes was *NanoTek* > *NanoShield* > *metals basis*. This extent of interaction was inversely related to the ZnO particle size where the *metals basis* nanoparticles were strongly aggregated. The contribution of the non-ionic dispersant added by manufacturer to the *NanoTek* and *NanoShield* interaction was uncertain. (2) Freshly prepared aqueous *Nanosun* ZnO nanoparticle (~25 nm) dispersions interacted with and penetrated DOPC coated Hg electrodes. Aggregation of the nanoparticles, coating of the ZnO with phosphate and coating of the ZnO with fulvic acid minimised ZnO-DOPC interaction. (3) *In-house* synthesised ZnO nanoparticles of lower primary particle size (~6 nm) than *Nanosun* ZnO nanoparticles interacted strongly with DOPC coated Hg electrodes with no evidence of penetration of the nanoparticle in the DOPC monolayer. Even after considerable aggregation of the particle to between 1 and 10 μm a strong interaction of the *in-house* synthesised ZnO with DOPC was observed.

Keywords: Zinc oxide nanoparticles; Phospholipid monolayers; Rapid cyclic voltammetry; Particle size; Particle aggregation.

1. Introduction

The increasing use of engineered nanoparticles has given rise to heightened concern for their biological activity and environmental impact [1]. Nanoparticles in aqueous dispersions have dimensions and properties in between those of micrometer-sized particles and dissolved compounds [2]. Their thermodynamics, transport, mechanical and chemical properties are dependent on their dimensions, and their large surface area generates considerable surface activity. Because of this, nanoparticles become highly active even if they are made of an inert material. In addition, the biological impact of nanoparticles depends on their size and structure in the solution environment as well as on their functionality because a small cluster of metal atoms can have a different chemical potential than the bulk solid and is more easily dissolved [3]. Another possible consequence of the large surface to volume ratio of nanoparticles is that during their transport they release a concentration of adsorbed surface species which itself may be toxic. This, coupled with the putative ability of nanoparticles to cross cell membranes and enter cells because of their small size [4], will enable them to release dissolved toxic species into the cell interior. Taking into account the full complexity of a nanoparticle's toxicity, an initial step in the study of their biological activity can involve an investigation into the interaction of the particles with and/or permeation into the cell membrane as the primary interface of a biological organism with the surrounding environment.

A study of the interaction of nanoparticles with cell membranes can be carried out on cell cultures or microorganisms but in these systems, there are more variables that can lead to a more elaborate analysis of the mechanisms involved. Another strategy in carrying out nanoparticle/cell membrane interaction studies is with model membrane systems based on the phospholipid bilayer backbone of the cell membrane such as liposomes. In fact a membrane model is used in the present study and is more manipulable than living cells in facilitating a rapid and controlled study of nanoparticle interaction with the phospholipid assemblies. In this article, the nanoparticle/biomembrane interaction was studied using a phospholipid monolayer on a mercury (Hg) film electrode. This is a powerful membrane model [5] that has been developed for *on-line* high-throughput application [6] and is custom designed for investigating phospholipid layer interactions. The system of phospholipids (usually dioleoyl phsphatidylcholine,DOPC) on a Hg electrode is an established biomembrane model used by leading workers in the field [7−10]. This model has shown similar results with peptide−phospholipid [11] and cholesterol−phospholipid [12,13] interactions to those obtained using the classical biomembrane models of free-standing bilayers and vesicles. Moreover, the monomolecular gramicidin channel in the monolayer on Hg [14,15] was shown to function in a very similar way to the bimolecular gramicidin channel in phospholipid bilayers. The indications are therefore that Hg has a minimal effect on the fluidity of the phospholipids, and hence the lipid layer's properties are very similar to those of the outer leaflet of free-standing bilayers and vesicles. The main difference in this system with respect to the phospholipid structure in a biological membrane is that the phospholipids form a monolayer on the Hg surface in the absence of an electric field whereas the phospholipid assembly in a biological membrane is always a bilayer. However, any biological membrane activity is initiated from the interaction at the phospholipid/water interface, which is the same in both a phospholipid monolayer and a bilayer system. The studied model draws its unique properties from the atomically smooth nature of the Hg surface, which has a minimal influence on the phospholipid layer's properties compared to phospholipid layers on solid electrodes, which have a significant effect on the layer's properties.

Two earlier studies have investigated the activity of polymeric [16] and SiO_2 [17] nanoparticles towards the phospholipid monolayer on Hg system. The activity of SiO_2 nanoparticles on the monolayer as an example of inorganic nanoparticles is inversely related to their particle size and the data could be explained as related to the effectiveness of the SiO_2 packing enabling maximum contact between the SiO_2 particle and phospholipid surface to be obtained. This reported study extends the investigation to ZnO nanoparticles which possess interesting properties enabling studies of their activity to lipid layers particularly challenging. In contrast to SiO_2 which is amorphous, ZnO is crystalline and polar [18]. ZnO shows a tendency to dissolve in aqueous dispersion and release free Zn^{2+} ion [19]. Finally ZnO nanoparticles have a strong tendency to aggregate [20,21].

ZnO is a semiconductor material which has many applications in industry. This has led to ZnO nanomaterials being used in the production of sunscreens [22], solar cells [23-25], electroluminescent devices [26], electrochromic windows [27], chemical sensors [28–30] and for functional coating formulations to protect wood, plastics and textiles from UV and microbial degradation [31, 32]. This increased use of ZnO nanoparticles results in increased perceived health and environmental risks. The small size of nanoparticles leads to both greater mobility and higher activity to biological membranes [33], which includes stronger binding to [34], and permeability within [35] the biological membrane. The biological activity of ZnO nanoparticles has been confirmed by a number of research articles [36,37]. At present an understanding of the factors in the toxicity of ZnO nanoparticles is rather ambiguous. It is not clear whether the toxicity of the ZnO arises from the Zn^{2+} which is released from ZnO [36] and known to be toxic and/or from the ZnO particle itself. A study into the affinity of ZnO particles for representative biological molecules would help explain whether the ZnO particle is directly implicated in any toxic event. To attempt to answer this, the current paper reports a study on the influence of ZnO nanoparticles on the phospholipid (DOPC) monolayer coated Hg film electrode. The ability of the nanoparticles to adsorb on and penetrate the phospholipid monolayer was studied and the effect of the size and functionality of the nanoparticles on the interaction was investigated. The DOPC monolayers are interrogated electrochemically using rapid cyclic voltammetry (RCV) comprised of a fast negative or cathodic going voltage ramp followed by a fast positive or anodic going voltage ramp both traversing a voltage excursion. The recorded current is directly proportional to the capacitance of the layers. Interaction of the nanoparticles with the layers is shown by a depression in two consecutive current peaks which are representative of two consecutive negative potential induced phospholipid phase transitions respectively[16,17]. Penetration of the DOPC layers by the nanoparticles gives rise to an increase in the capacitance current value of the monolayer [16].

2. Experimental

2.1. Materials

All ZnO nanoparticle concentrations are expressed as weight per volume except where stated. The ZnO nanoparticles used are displayed in Table 1. 1,2-Dioleoyl-*sn*-glycero-3-phosphocholine (DOPC) was obtained from Avanti Polar Lipids (Alabaster, US) and was of >99% purity. All other reagents were of analytical grade and purchased from SigmaAldrich.

Table 1. ZnO nanoparticle (NP) characteristics

ZnO brand	*metals basis*	*NanoShield*	*NanoTek*	*Nanosun*	*in-house*
Source	*Alfa Aesar*	*Alfa Aesar*	*Alfar Aesar*	Micronisers	*synthesised*
Available form	*powder*	*dispersion*	*dispersion*	*powder*	*dispersion*
NP 1^0 diam, nm (TEM)	*45±30*	*70 ± 43*	*55 ± 30*	*25±1.1*	*6.2±0.3*
NP, aqueous dispersion diam, nm (DLS)	*>2000*	*331 ± 87*	*80 ± 17*	*86.7±9.2*	*22.8±1.3*

2.2. Methods

2.2.1. Electrochemical flow system setup

The flow system has been described previously [17] and consisted of: (i) a peristaltic pump (Cole-Parmer instrument co. Cat N. 7554-20), (ii) two universal valve switching modules (Anachem Ltd.), (iii) a 10 dm^3 electrolyte reservoir, (iv) 25 cm^3 sample cell, (v) two magnetic stirrers for stirring of solution in electrolyte reservoir and sample cell, and (vi) a flow cell. All parts were connected to each other by teflon and silicon tubing. The flow cell was made from plexiglass with silicon rubber sealing. A REF201 Red Rod Ag/AgCl 3.0 mol dm^{-3} KCl reference electrode (VWR international Ltd.) was fitted into the cell and all potentials in this paper unless otherwise stated are quoted versus the potential of this electrode. Silicon wafer-based microfabricated Pt electrodes (Tyndall National Institute, Ireland) were inserted into the flow cell. These electrodes consisted of eight Pt discs with diameter of 1 mm and two Pt rectangles of 8.3 mm long and 1.8 mm wide embedded on a 28 by 28 mm^2 diced silicon wafer substrate possessing a surface of 0.2 µm dry silicon oxide. Each Pt area was connected to respective contact pads by a 0.5 mm thick Pt trace interconnect which was insulated with approximately 1.5 mm of Si_3N_4 deposited by plasma enhanced chemical vapour deposition (PECVD). The microfabricated Pt electrode was connected to an Autolab potentiostat, PGSTAT 30 (Ecochemie, Utrecht, Netherlands) interfaced to a Powerlab 4/30 signal generator (AD Instruments Ltd.) controlled by Scope™ software. The volume of the flow cell was 0.15 cm^3. The flow system was used in four different settings depending on the positions of valves, these were as follows:

1. Electrolyte was drawn from an electrolyte reservoir and discharged to waste after passing through flow cell;
2. Electrolyte was drawn from electrolyte reservoir and filled the sample cell;
3. Electrolyte was drawn from sample cell and discharged to waste after passing through flow cell;
4. Electrolyte was drawn from sample cell, passed through flow cell and re-entered into the sample cell by cycling. All solutions were constantly purged with argon (Air Products) during all electrochemical experiments.

A schematic of the flow system is depicted in Fig 1 which allowed for DOPC deposition and removal and RCV measurements to be carried out with electrolyte from the electrolyte cell and exposure of DOPC to the sample from sample cell by a simple switching of valves. This method of flow control enables only adsorbed species **(not dissolved or dispersed species)** to be measured by RCV on the DOPC coated and uncoated Hg.

2.2.2. Electrode pretreatment and RCV

Electrodeposition of Hg on to Pt disc electrodes was performed in the flow cell [17]. The working electrodes were cleaned prior to electrodeposition in a hot solution of H_2SO_4 (Fisher Scientific) and 30% H_2O_2 (Fluka) mixture in a ratio of approximately 3:1, respectively and rinsed with Milli-Q 18.2MΩ (Millipore UK) water before drying under nitrogen (N_2). The reduction of Hg^{2+} to Hg on the Pt disc was performed at −0.4 V and monitored by means of chronocoulometry with a cut-off value for the charge (Q) flowed of 1 C per electrode under constant flow rate 5 cm^3 min^{-1} of 50 mmol dm^{-3} $Hg(NO_3)_2$ solution circulating through the flow cell. Once the designated amount of charge had passed, the circuit was opened and the electrode was washed by constant flow of 5 cm^3 min^{-1} of MilliQ 18.2MΩ (Millipore UK) water for 30 min. The Pt electrodes with electrodeposited Hg are subsequently referred to as Pt/Hg electrodes throughout the text. Rapid cyclic voltammetry (RCV) was carried out in 0.1 mol dm^{-3} KCl (previously calcined at 600°C) solution at pH 6.8-7.2. The KCl solution in the electrolyte reservoir was de-aerated by purging with argon (Air Products) for 60 min before use. 20 cm^3 of this electrolyte was drawn into the sample cell prior to each experiment and de-aerated by purging with argon (Air Products) for 5 min. The electrochemical cell and screened cables were contained in a Faraday cage. The electrodes were connected to the Autolab potentiostat as described above. The RCV voltage excursion was from −0.4 V to potentials between -1.125 and -3.0 V depending on the application at a scan rate of 40 V s^{-1}. Scans were repeated continuously or with an interval of 1 s between each scan.

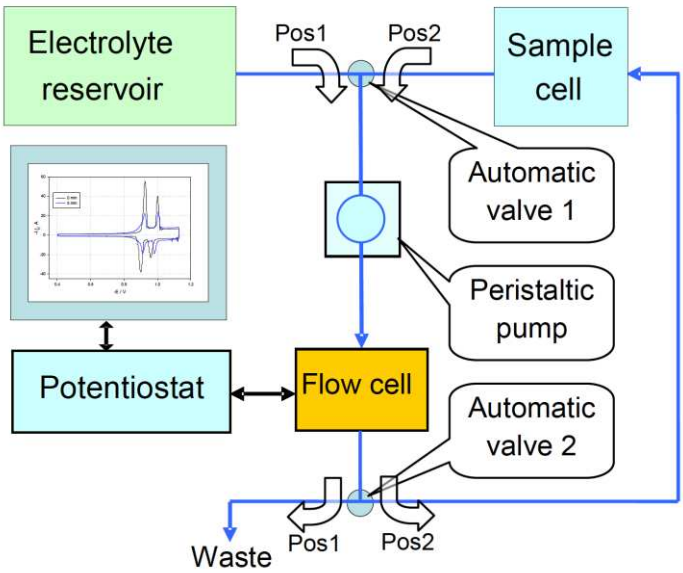

Figure 1. Schematic view of flow system.

2.2.3. Synthesis of *in-house* ZnO nanoparticles.

ZnO nanoparticles were chemically synthesised from LiOH and $Zn(Ac)_2$ in non-aqueous conditions according to procedure [38]. 1 dm^3 of 0.14 mol dm^{-3} LiOH ethanol solution was added to 1 dm^3 of finely ground 0.1 mol dm^{-3} anhydrous $Zn(Ac)_2$ ethanol dispersion at 4°C. Stirring for 5 min resulted in the formation of a transparent solution. The reaction mixture was incubated at 4 °C for 3 days. Following this, the resultant ZnO nanoparticle dispersion was tested by Dynamic Light Scattering (DLS) and mixed with pentane in ratio 1:10 leading to precipitation of the ZnO nanoparticles which were then washed with pentane and stored as a 100 g dm^{-3} ZnO in pentane dispersion. Prior to use the dispersion was mixed with absolute ethanol in ratio 1:5. Excess of pentane and some ethanol was dried out by stream of nitrogen. The ZnO in ethanol dispersion was diluted by ethanol to concentration of 40 g dm^{-3}. Freshly made ZnO ethanol dispersion was diluted with Milli-Q 18.2MΩ (Millipore UK) water in ratio 1:10 and the resultant dispersion was stable for 1 hour before aggregation was evident. This dispersion was used for RCV experiments by addition to the electrolyte solution.

2.2.4. Electrochemical characterisation of interactions.

The flow system was set up with valves 1 and 2 at position 1 (see Fig 1) and the flow rate was set to 10 cm^3 min^{-1}. RCV was initiated continuously at a voltage excursion from -0.4 to -3.0 V. 100-200 µL of DOPC in MillQ water dispersion (0.2 mg cm^{-3}) was injected into the flow cell and after 1-2 seconds when the characteristic voltammetric peaks of DOPC appeared, RCV was terminated. In case of bare mercury studies, the DOPC suspension was not added into the cell and the electrode remained clean. RCV was then initiated again with a voltage excursion from -0.4 to -1.625 V to test the quality of the DOPC monolayer as indicated by a maximum height of the voltammetric peaks. If the quality of the DOPC monolayer was found not to be acceptable as shown by depressed voltammetric peaks then the procedure for coating was repeated. The control monitoring RCV scan was initiated with a voltage excursion from -0.4 to -1.125 V at 40 V s^{-1} and saved for future analysis as an initial curve. Following successful DOPC deposition, the flow rate was set to 10 cm^3 min^{-1}. Valve 2 was switched from position 1 to position 2 until the electrolyte filled the sample cell to 20 cm^3 and then the valve 2 was switched to position 1 again. An aliquot of ZnO nanoparticle dispersion was injected into the sample cell to the required concentration using a glass syringe. In case of nanoparticle dispersion tests with added phosphate buffer or fulvic acid, the sample cell was filled separately with solutions containing 0.1 mol dm^{-3} KCl with 0.01 mol dm^{-3} of potassium phosphate buffer (pH 7.4) or 5 mg dm^{-3} of fulvic acid respectively. Valve 1 was then immediately switched to position 2. After 30 seconds, valve 2 was switched to position 2 and measurements continued for 5-20 min depending on interaction rate. The RCV was adjusted to a voltage excursion from -0.4 to -1.125 V at 40 V s^{-1} at a scan repetition rate of 1 scan s^{-1} during the entire ZnO dispersion exposure time. At the end of the exposure, the valves were switched to position 1 in order to remove all ZnO nanoparticles and dissolved Zn (II) and the measurement RCV scan was collected and saved for future analysis as a final plot. Subsequently the sample cell was emptied and the system was washed by sequential switching of valves between positions 1 and 2. The Pt/Hg electrode was electrochemically cleaned *in situ* by repetitively cycling its potential from −0.4 to −3 V at 80 V s^{-1} with an electrolyte flow rate of 10 cm^3 min^{-1} and the valves set to position 1 for 30-60 s until the current peaks relating to absorbed material on the Hg surface disappeared. This cleaning procedure has been previously described in detail [6].

2.2.5. Dynamic light scattering (DLS) study of ZnO nanoparticle dispersions

25 µL of a 40 g dm^{-3} dispersion of ZnO nanoparticles was added to 1 cm^3 of Milli-Q 18.2MΩ (Millipore UK) water, sonicated in a Branson 1200 ultrasonic bath sonicator for 1 min and the size of the nanoparticle aggregates was measured by DLS on a nanoZS zetasizer (Malvern Instruments Ltd).

2.2.6. Stability of ZnO nanoparticle dispersions

The degree of aggregation of all ZnO nanoparticles in different solutions was studied in independent experiments by DLS. ZnO nanoparticle dispersions were tested for stability in 0.1 mol dm^{-3} KCl solution. In a typical experiment 10 µL of a 40 g dm^{-3} dispersion of ZnO nanoparticles was added to 1 cm^3 of Milli-Q 18.2MΩ (Millipore UK) water, sonicated in a Branson 1200 ultrasonic bath sonicator for 1 min and the size of the nanoparticle aggregates was measured by DLS on a nanoZS zetasizer (Malvern Instruments Ltd). 33.3 µL of 3 mol dm^{-3} KCl solution was then added to the nanoparticle dispersion to give approximately 0.1 mol dm^{-3} KCl solution, shaken and measured using DLS every 10 s.

2.2.7. Transmission Electron Microscopy (TEM)

The ZnO nanoparticle dispersion was diluted down to about 0.12 % concentration and drop caste on to holey carbon coated copper TEM grid (Agar Scientific). After the sample was dried it was examined in a Philips CM200 FEGTEM Field emission gun TEM/STEM with Supertwin Objective lens.

3. Results and discussion

In the results from the experiments with commercially sourced ZnO nanoparticle preparations, it is observed that only the *NanoTek* and *NanoShield* dispersions effect an interaction with the DOPC coated Pt/Hg. These interactions, which are similar to those of SiO_2 nanoparticles with DOPC [17], are manifest as a significant depression of the capacitance current peaks on the RCV. Fig 2(a) summarises the results as a percentage depression of one of the capacitance current peaks at potential ~ -0.95V. DLS data (Fig 2(b)) indicates that the particle size of the dispersions inversely correlates with the extent of interaction of these dispersions with the DOPC coated Hg. The *metals basis* ZnO which is highly aggregated with particle size >1mm exhibits no significant interaction whereas the *NanoTek* dispersion with particle diameter of ~100 nm shows the strongest interaction. It is well documented [20,21] that pure ZnO nanoparticles are unstable in dispersion and show a strong tendency to aggregate as indicated by the behaviour of the *metals basis* sample. However the *NanoShield* and *NanoTek* dispersions are stabilised through the addition of a non-ionic dispersant by the supplier at source. The inverse relation between particle size and the extent of interaction of particle with DOPC layer has been noted previously for SiO_2 nanoparticles [17]. It remains uncertain however whether the effects of *NanoShield* and *NanoTek* ZnO on the DOPC layer are due to the dispersant in the ZnO sample or the nanoparticle itself or both. Because of this, further experiments were carried out with ZnO dispersions with no added dispersant obtained from:- (i) a supplier where the particle was sourced as a powder and the preparation had been well described (*Nanosun*) and, (ii) *in-house* synthesis. Fig 3(a) is a TEM image of the dry *Nanosun* particles where minimal aggregation is apparent and the primary particle diameter is ~ 25 nm. The DLS examination Fig 3(b) of *Nanosun* particles in 0.1 mol dm^{-3} KCl shows that initially some aggregation of these particles occurs to give aggregates of

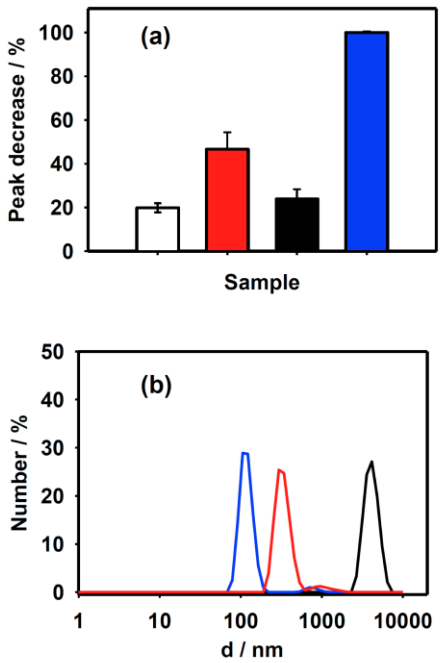

Figure 2. (a) % peak current decrease (relative to control prior to nanoparticle dispersion exposure) on cathodic arm of RCV (-0.4 to -1.125 V at scan rate 40 Vs^{-1}) in flow cell after 10 min interaction of DOPC coated MFE with the following named 0.1% ZnO nanoparticle dispersions in 0.1 mol dm^{-3} KCl: without nanoparticle dispersion (white column); *NanoShield* (red column); *metals basis* (black column) and *NanoTek* (blue column). (b) DLS number particle size distribution of 0.1%: *metals basis* (black line), *NanoShield* (red line) and *NanoTek* ZnO (blue line) in MilliQ water.

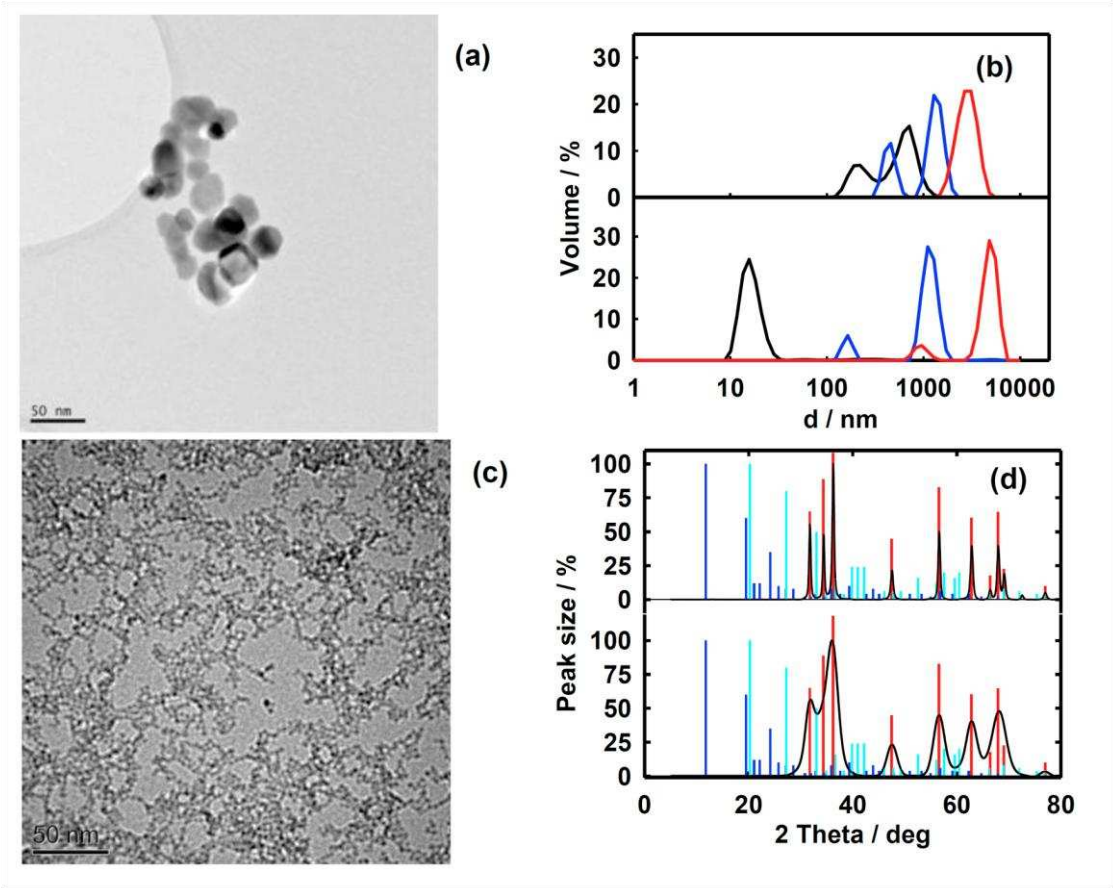

Figure 3. (a) TEM image of *Nanosun* nanoparticles (NP). (b) Volume particle size distribution of *Nanosun* (top) and *in-house* (bottom) ZnO NP in 0.1 mol dm^{-3} KCl at times 0 s (black line), 20 s (blue line), and 120 s (red line). (c) TEM image of *in-house* ZnO NP. (d) XRD spectra of *Nanosun* (top, black), *in-house* (bottom, black) ZnO. ZnO (hexagonal wurtzite crystal structure) (red bars), $Zn(Ac)_2$ (blue bars) and $Zn(OH)_2$ (cyan bar).

diameters between 100 and 1000 nm. This aggregation continues till at 3 minutes the secondary particle diameter is between 1 and 10 μm. A TEM image of *in-house* synthesised ZnO nanoparticles dried from MilliQ water dispersion is displayed in Fig 3(c). The primary particle size is ~6 nm. The DLS plot of an *in-house* synthesised ZnO dispersion in 0.1 mol dm^{-3} KCl at 0, 20 s and 120 s respectively is displayed in Fig 3(b). At 0 s the mean diameter is about 20 nm but this increases to diameters between 1 and 10 μm after 120 s. Fig 3(d) shows the XRD spectrum for *Nanosun* and *in-house* synthesised ZnO which is characteristic of pure ZnO (also shown) and is quite distinct from $Zn(OH)_2$ and $Zn(Ac)_2$. The broad peaks associated with *in-house* synthesised ZnO are related to its smaller primary particle size. The full width at half maximum peak intensity, peak position and wavelength of the XRD peaks can be used for calculation of crystallite particle size. Using the Scherrer equation [39] we calculated 6.2 nm crystallite size for *in-house* synthesised ZnO nanoparticles and 30 nm crystalline size for Nanosun ZnO nanoparticles.

Exposure of the DOPC layers to a 0.4% dispersion of ZnO *Nanosun* nanoparticles elicited a significant change in the RCV curve (Fig 4(a)). This was manifest as a decrease in height of capacitance current peaks and an increase in the capacitance current as a

function of negative potential from potential -0.7 V. It is very significant that after incubating the ZnO dispersion in 0.1 mol dm^{-3} KCl for 30 minutes which promotes the particle aggregation as shown in Fig 3(b), the interaction with the DOPC as seen from the effect on the RCV plot is much decreased (Fig 4(b)). A similar decrease in the effect of the ZnO dispersion on the RCV plot is observed when the experiment is carried out with a ZnO dispersion prepared in 0.1 mol dm^{-3} KCl with added 0.01 mol dm^{-3} of potassium phosphate buffer (pH 7.4) (Fig 4(c)) or added 5 mg dm^{-3} fulvic acid (Fig 4(d)) respectively. The phosphate in the buffer reacts with Zn^{2+} released by ZnO to form $Zn_3(PO_4)_2$. This coats the particles and suppresses interaction with the phospholipids. Similarly, fulvic acid is surface active and coats the particles decreasing the particle's activity towards the DOPC layers. Fulvic acid as a component of natural organic material is known to adsorb on ZnO nanoparticles [21] and indeed metal oxides in general [40].

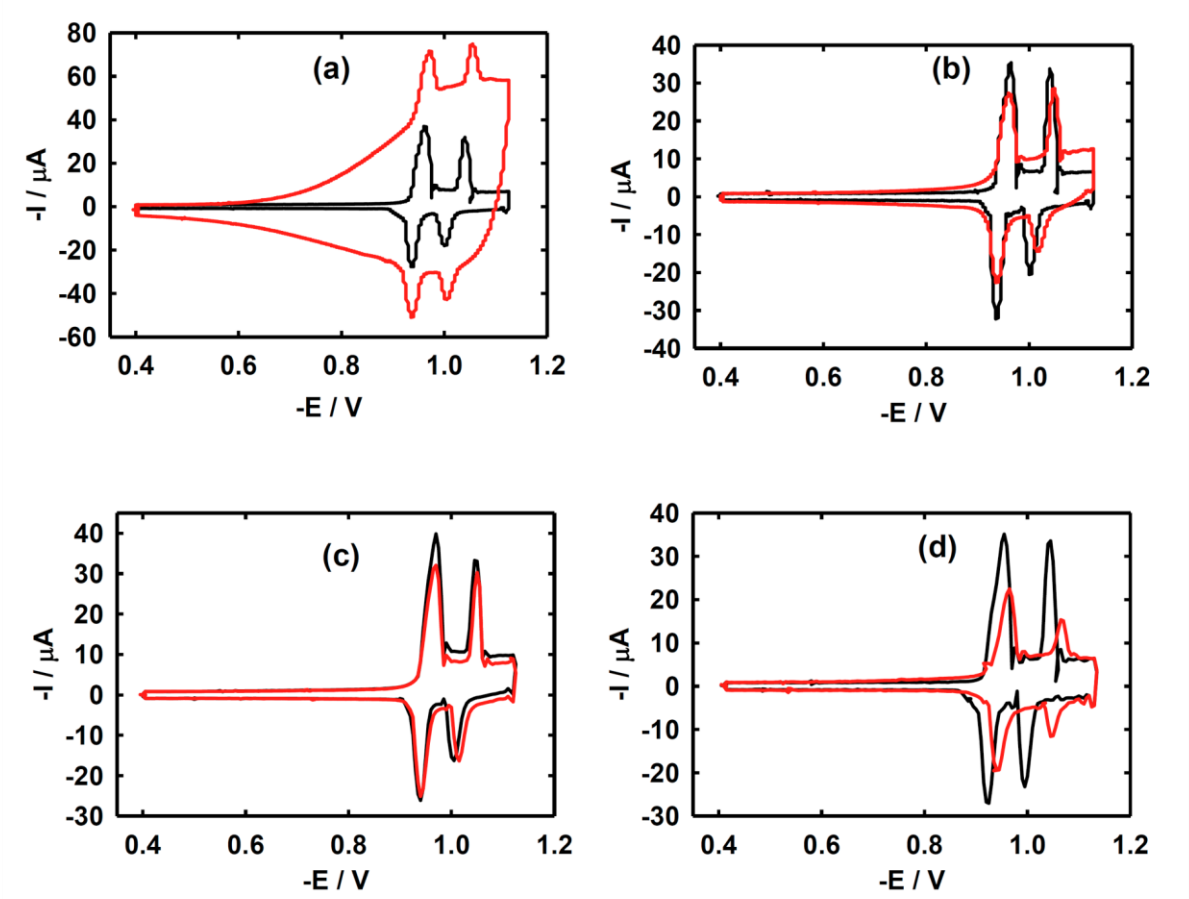

Figure 4. (a) and (b) RCV of DOPC coated MFE following exposure to *Nanosun* ZnO: (a) freshly dispersed, and (b) aged for 30 minutes, in 0.1 mol dm^{-3} KCl. (c) and (d) RCV of DOPC coated MFE following exposure to *Nanosun* ZnO dispersion in 0.1 mol dm^{-3} KCl (c) with 0.01 mol dm^{-3} of phosphate buffer (pH 7.4) and (d) with added 5 mg dm^{-3} fulvic acid. In all graphs RCV (scan rate 40 Vs^{-1}) carried out before (black line) exposure to 0.4% ZnO dispersion and after (red line) exposure to 10 min of flow of 0.4% ZnO dispersion.

Experiments carried out with the *Nanosun* and *in-house* synthesised ZnO dispersion in 0.1 mol dm^{-3} KCl at an uncoated Hg electrode and with $ZnCl_2$ on a DOPC uncoated and

coated electrode are displayed in Fig 5. The interaction of freshly dispersed (Fig 5(a)) and aggregated (Fig 5(b)) *Nanosun* ZnO with uncoated Hg leads to an increase in the capacitance current on the RCV plot as a function of negative potential from potential -0.6 V. This current is decreased by about 20-30% following aggregation of the ZnO particles (Fig 5(b)). The interaction of freshly dispersed and aggregated *in-house* synthesised ZnO with Hg (see Figs 5(a) and (b)) is similar albeit with a differing current-voltage profile. Indeed a slight increase in capacitance current is seen following aggregation. These results can be interpreted in the following way. ZnO particles adsorb on uncoated Hg and contribute to the capacitance current. The capacitance current can be related to a charging of adsorbed semi-conductor ZnO particles through the injection of electrons therein [41]. The increase in capacitance current takes place at potentials more positive than those associated with reversible soluble Zn^{2+} reduction on Hg (~ -1.0 V [42]). The voltammetric results of ZnO particles on uncoated Hg indicate that the capacitance

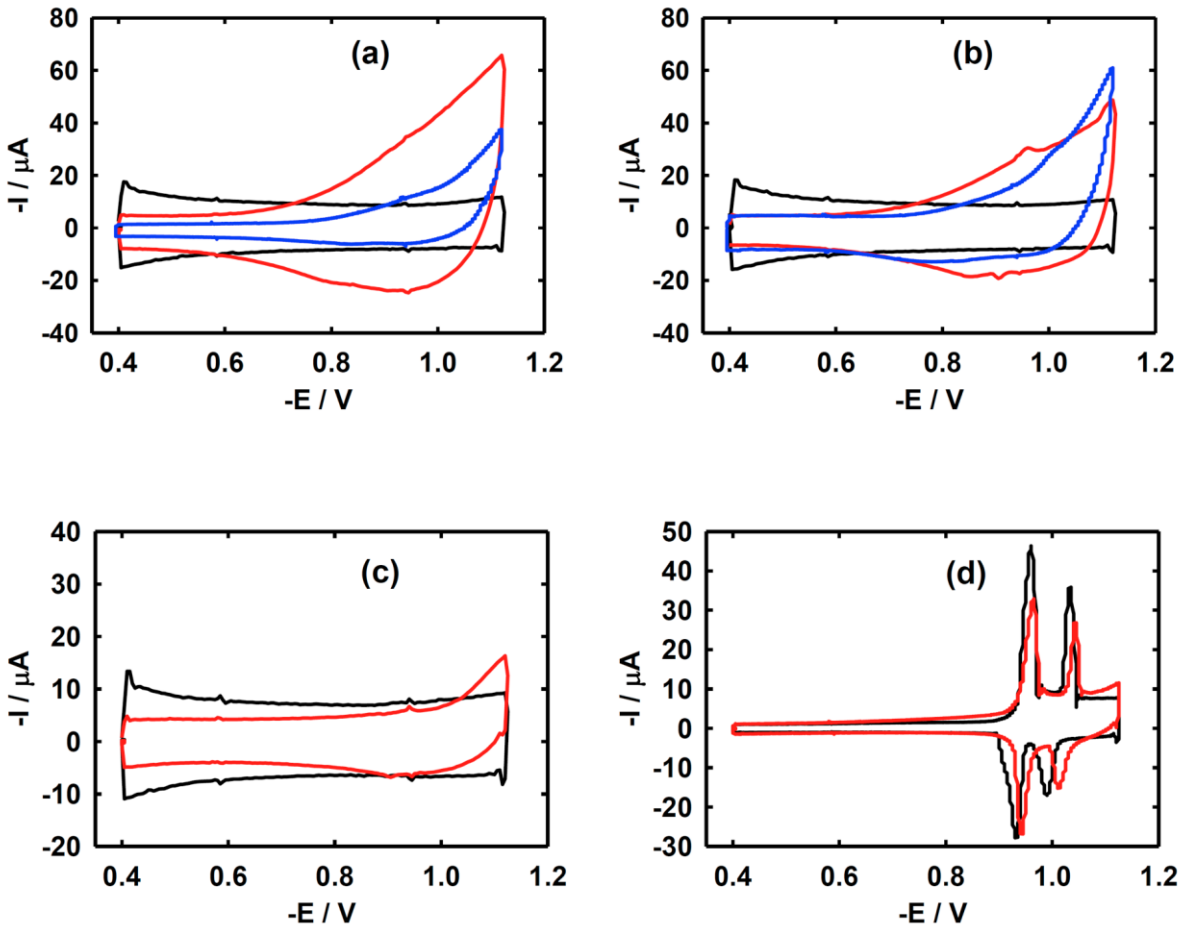

Figure 5. (a), (b), RCV (scan rate 40 Vs^{-1}) of uncoated MFE in 0.1 mol dm^{-3} KCl before (black line) and after (red and blue lines) exposure to 0.4 % *Nanosun* ZnO (red line) and 0.4% *in-house* synthesised ZnO (blue line) (a) freshly dispersed and (b) aged for 30 mins in 0.1 mol dm^{-3} KCl, (c) and (d) RCV of DOPC (c) uncoated, and (d) coated MFE in 0.1 mol dm^{-3} KCl before (black line) and after (red line) exposure to 0.01 mol dm^{-3} $ZnCl_2$.

current increase which is observed following interaction of *Nanosun* ZnO with DOPC coated Hg (see Fig 4(a)) shows that ZnO nanoparticles have penetrated the monolayer allowing electron transfer from the Hg to the semi-conductor ZnO particles within the DOPC layer. It is significant that the current-voltage profile is not directly identical to that of the uncoated Hg electrode in presence of *Nanosun* ZnO. This shows that the electron transfer is sensitive to the environment of the nanoparticles. Such an effect would be expected from properties of semiconductor nanoparticles where surface effects dominate the electron transfer characteristics [43]. Interestingly the difference between the current-voltage traces for the unaggregated (Fig 5(a)) particles and aggregated (Figs 5(b)) particles on uncoated Hg is one of current magnitude. On the other hand the current is marginally shifted to negative potentials in the RCVs of the *in-house* ZnO nanoparticles of smaller primary size. The origin of these differences are not as yet understood although it has been shown that the electron transfer to semi-conductor CdTe particles depends on the CdTe particle size [44-6] and nanoparticle size in general [47]. It was predicted that the electron transfer to smaller particles is shifted to more extreme potentials. The reason for this is that the top of the particle valence band is shifted towards lower energies and the bottom of the conduction band is shifted to higher energies with decreasing particle size. A similar process could account for the differing current-voltage traces for the two groups of particle dispersions of different primary particle diameter respectively

Fig 5(c) displays the effect of 0.01 mol dm^{-3} $ZnCl_2$ solution on the current-voltage curve of Hg electrode. A small decrease in current is observed with a small increase in current at potentials more negative than -1.0 V. The small decrease in current could be related to the adsorption of Zn(II) species from the 0.01 mol dm^{-3} $ZnCl_2$ on the Hg electrode and the small increase of current at negative potentials is associated with the reduction of these adsorbed Zn(II) species. The effect of exposing the DOPC coated electrode to 0.01 mol dm^{-3} $ZnCl_2$ on the current-voltage curve is small with a slight capacitance current peak depression (Fig 5(d)). Conclusions from these results are that exposure of uncoated and DOPC coated Hg to soluble $ZnCl_2$ has little effect on the capacitance-voltage curves. This shows that the response of the uncoated and DOPC coated electrode to ZnO nanoparticle dispersions is mediated primarily through particle interaction and not through soluble Zn^{2+} interaction associated with the particle dispersion.

In Figs 6(a), (b) and (c) the influence of the 0.4% *in-house* ZnO dispersions on the DOPC coated Hg electrode is displayed. The effect of the freshly prepared *in-house* synthesised ZnO with DOPC at t=0 s is to totally suppress the capacitance current peaks. A similar response of the DOPC coated Hg to the 30 minute 0.1 mol dm^{-3} KCl incubated ZnO nanoparticle dispersion is observed (Fig 6(b)). After 9 hours incubation of the ZnO in 0.1 mol dm^{-3} KCl the activity of the ZnO nanoparticle dispersion towards the DOPC coated Hg is considerably decreased (Fig 6(c)). In the interaction of the *in-house* synthesised ZnO nanoparticles with the DOPC coated electrode no increase in the baseline capacitance current is seen in contrast to the response of the coated electrode to the *Nanosun* particles. The results in Fig 6 show therefore that the ZnO with smaller primary particle size is very much more active towards the DOPC than the larger *Nanosun* particles.

The effect of both *Nanosun* (Figs 4(a),((b)) and *in-house* particles (Figs 6(a),(b),(c)) on the DOPC coated electrode can be compared with the results of the effect of the same particles on uncoated Hg (Figs 5 (a), (b), (c) and (d)). It can be seen quite clearly that current-voltage traces from the RCV of the coated electrode are recording the influence of the primary particle size and the aggregation state of the ZnO particles only on the ZnO-DOPC interaction. Interestingly both the *Nanosun* and *in-house* synthesised ZnO are

aggregated to similar extents after 120 s incubation in 0.1 mol dm^{-3} KCl (see Fig 3(b)) yet even after 30 minutes incubation, the *in-house* synthesised ZnO shows greater activity towards the DOPC coated Hg than that of the *Nanosun* particles. It can only be concluded therefore that the interaction of ZnO nanoparticles with DOPC depends to some extent on the primary particle size although after nine hours incubation in 0.1 mol dm^{-3} KCl, interaction of *in-house* synthesised ZnO nanoparticles with DOPC is decreased. Of most interest is that the *in-house* ZnO does not effect an increase in the capacitance current at potentials more positive than those characterising the current peaks. This indicates that these particles do not penetrate the DOPC monolayer irrespective of their aggregation state. The release of Zn^{2+} by *Nanosun* and *in-house* synthesised ZnO particles has been studied in a previous paper. It has been shown that the extent of Zn^{2+} release is dependent on the ZnO primary particle size [19,48]. This is commensurate with the classical predictions from the Kelvin equation relating solubility to the curvature of the particle. The fact that the solubility was unaffected by the aggregation state shows that the aggregates are a relatively loose conglomerations of particles. This has been borne out by the present study where the interaction of the ZnO particles with DOPC monolayers appears to be partially dependent on their primary size. The strong tendency of ZnO particles to aggregate has been related to their solubility [49] in that the soluble Zn (II) species adsorb on the ZnO particles and screen the surface potential leading to the attractive van der Waals forces betwwen particles to predominate. In this way the smaller ZnO particles show a stronger tendency in water to aggregate. The lack of penetration of the smaller ZnO particles into the DOPC could be related to their smaller physical size and stronger interaction with the polar heads of the DOPC.

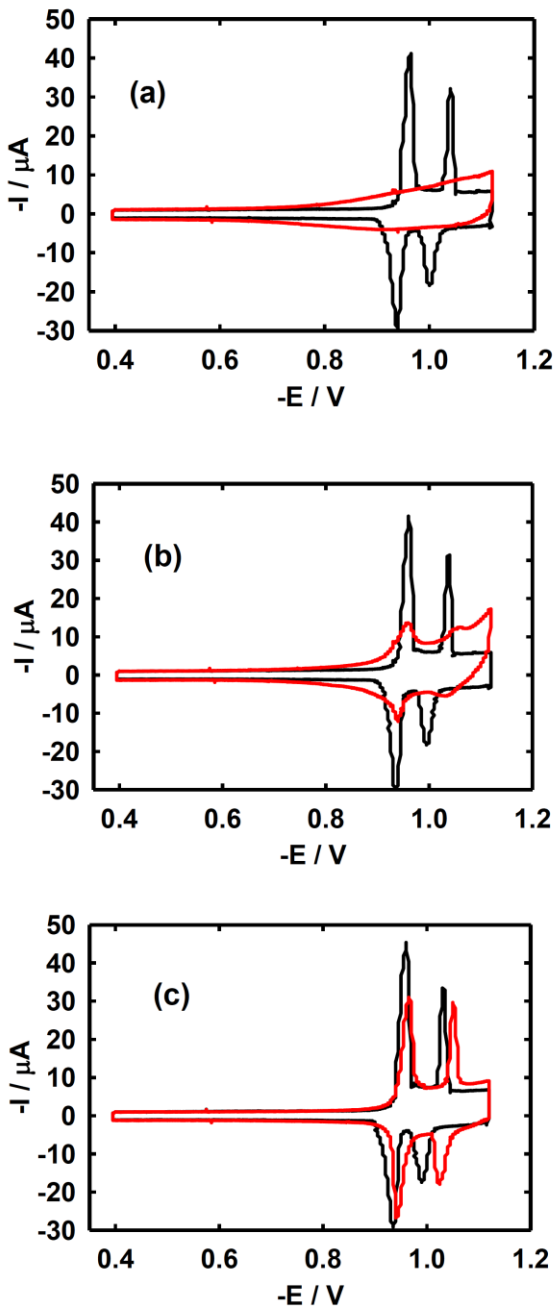

Figure 6. RCV (scan rate 40Vs^{-1}) of DOPC coated MFE in 0.1 mol dm^{-3} KCl before (black line) and after (red line) 10 mins exposure to:- 0.4% *in-house* synthesised ZnO in 0.1 mol dm^{-3} KCl (a) freshly dispersed (b) aged for 30 mins and, (c) aged for 9 hours.

Conclusions

1. The order of interaction of common commercially sourced ZnO nanoparticles with DOPC coated Hg electrodes was *NanoTek* > *NanoShield* > *metals basis*. This extent of interaction was inversely related to the ZnO particle size where the *metals basis* nanoparticles were strongly aggregated. The contribution of the non-ionic dispersant to the *NanoTek* and *NanoShield* -DOPC interaction is uncertain.
2. Freshly prepared aqueous *Nanosun* ZnO nanoparticle (~25 nm) dispersions interacted with and penetrated DOPC coated Hg electrodes. (i) Aggregation of the nanoparticles, (ii) coating of the ZnO with phosphate and, (iii) coating of the ZnO with fulvic acid minimised ZnO-DOPC interaction.
3. *In-house* synthesised ZnO nanoparticles of lower primary particle size (~6 nm) than *Nanosun* ZnO nanoparticles interacted strongly with DOPC coated Hg electrodes with no evidence of penetration of the DOPC monolayer. Even after considerable aggregation of the particle to between 1 and 10 mm a strong interaction of the ZnO with DOPC was observed.
4. Both *Nanosun* and *in-house* synthesised ZnO nanoparticles adsorb on uncoated Hg electrodes. Voltammetry showed an electron transfer to the semi-conductor ZnO particles, the extent of which was dependent on magnitude of applied negative potential.
5. Although a phospholipid monolayer has been used in this study, more biologically relevant biological studies may be carried out with bilayers. However the interaction of the ZnO particles with the DOPC takes place at the DOPC/solution interface which is identical for a bilayer and monolayer. In addition other studies have shown that the interactions of SiO_2 particles with a monolayer and bilayer and the energetics thereof are identical [17,50]. Stable bilayers of DOPC can now be prepared on the fabricated Pt/Hg electrode (A.V. Vakurov in preparation) and these systems will be used to study particle-phospholipid interactions in future studies.

Acknowledgements

This work was part of the ENNSATOX programme funded by EU FP7 under grant agreement no. NMP-229244. The work was also funded by the 2008 Brian Mercer Award from the UK Royal Society. GML was funded by a Nuffield Foundation Bursary.

References

[1] Hapeman C J Dionigi C P Zimba and P V, McConnel L L 2002 Agrochemical and Nutrient Impacts on Estuaries and Other Aquatic Systems *J. Agric. Food Chem.* 50 4382-4384

[2] Schmid G (Editor) 2004 *Nanoparticles: From Theory to Application* (Wiley-VCH Verlag GMBH)

[3] Liu W T 2006 Nanoparticles and their biological and environmental applications *Journal of Bioscience and Bioengineering* 102 1-7

[4] Lok C N Ho C M Chen R He O Y Yu W Y Sun H Tam P K Chiu J F and Che C M 2006 Proteomic analysis of the mode of antibacterial action of silver nanoparticles *J Proteome Res*. 5 916-924

[5] Coldrick Z Steenson P Millner P Davies M and Nelson A 2009 Phospholipid monolayer coated microfabricated electrodes to model the interaction of molecules with biomembranes *Electrochimica Acta* 54 4954-4962

[6] Coldrick Z Penezic´ A Gasˇparovic B Steenson P Merrifield J and Nelson A 2011 High throughput systems for screening biomembrane interactions on fabricated mercury film electrodes *J. Appl. Electrochem.* 41 939-949

[7] Stoodley R Bizzotto D 2010 *Analyst* 128 552–561

[8] Moncelli M R Becucci L Buoninsegni F T and Guidelli R 1998 Surface dipole potential at the interface between water and self-assembled monolayers of phosphatidylserine and phosphatidic acid *Biophysical Journal* 74 2388–2397

[9] Mauzeroll J Buda M Bard A J Prieto F and Rueda M 2002 Detection of Tl(I) transport through a gramicidin−dioleoylphosphatidylcholine monolayer using the substrate generation−tip collection mode of scanning electrochemical microscopy *Langmuir* 18 9453-9461

[10] Becucci L Moncelli M R and Guidelli R 2003 Pore formation by 6-ketocholestanol in phospholipid monolayers and its interpretation by a general nucleation-and-growth model accounting for the sigmoidal shape of voltage-clamp curves of ion channels *J. Am. Chem. Soc.* 125 3784-3792

[11] Ringstad L Protopapa E Lindholm-Sethson B Schmidtchen A Nelson A and Malmsten M 2008 An electrochemical study into the interaction between complement-derived peptides and DOPC mono-and bilayers *Langmuir* 24 208-216

[12] Nelson A and Auffret N 1988 Phospholipid monolayers of di-oleoyl lecithin at the mercury/water interface *J. Electroanal. Chem.* 244 99-113

[13] Pasek M Brette F Nelson A Pearce C Qaiser A and Orchard C H 2008 Quantification of t-tubule area and protein distribution in rat cardiac ventricular myocytes *Progress in Biophysics & Molecular Biology* 96 244-257

[14] Nelson A 2001 Conducting gramicidin channel activity in phospholipid monolayers *Biophysical J.* 80 2694-2703

[15] Becucci L Moncelli M R and Guidelli R 2002 Thallous ion movements through gramicidin channels incorporated in lipid monolayers supported by mercury *Biophysical Journal* 82 852–864

[16] Ormategui N Zhang S Loinaz I Brydson R Nelson A and Vakurov A 2012 Interaction of poly (N-isopropylacrylamide)(pNIPAM) based nanoparticles and their linear polymer precursor with phospholipid membrane models *Bioelectrochemistry* 87 211-9.

[17] Vakurov A Brydson R and Nelson A 2012 Electrochemical modeling of the silica nanoparticle–biomembrane interaction *Langmuir* 28 1246−1255

[18] Schulz H and Thiemann K H 1979 Structure parameters and polarity of the wurtzite type compounds Sic—2H and ZnO *Solid State Communications* 32 783-785

[19] David C A Galceran J Rey-Castro C Puy J Companys E Salvador J Monne J Wallace R and Vakurov A 2012 Dissolution kinetics and solubility of ZnO nanoparticles followed by AGNES *Journal of Physical Chemistry C* 116 11758-11767
[20] Bian S-W Mundunkotuwa I A Rupasinghe T and Grassian V H 2011 Aggregation and dissolution of 4 nm ZnO nanoparticles in aqueous environments: influence of pH, ionic strength, size, and adsorption of humic acid *Langmuir* 27 6059-6068
[21] Zhou D and Keller A A 2010 Role of morphology in the aggregation kinetics of ZnO nanoparticles *Water Research* 44 2948-2956
[22] Smijs T G and Pavel S 2011 Titanium dioxide and zinc oxide nanoparticles in sunscreens: focus on their safety and effectiveness *Nanotechnology, Science and Applications* 4 95–112
[23] Law M Greene LE Johnson J C Saykally and R Yang P 2005 Nanowire dye-sensitized solar cells *Nature Materials* 4 456-9
[24] Zhang Q Chou T P Russo B Jenekhe S A and Cao G 2008 Aggregation of zno nanocrystallites for high conversion efficiency in dye- sensitized solar cells *Angew. Chem.* 120 2436-2440
[25] Galoppini E Rochford J Chen H Saraf G Lu Y Hagfeldt and A Boschloo G 2006 Fast electron transport in metal organic vapor deposition grown dye-sensitized ZnO nanorod solar cells *J.Phys.Chem. B* 110 16159-16161
[26] Park W I and Yi G-C 2004 Electroluminescence in n- ZnO nanorod arrays vertically grown on p- GaN *Adv. Mater.* 16 87-90
[27] Jin Z-C Hamberg I Granqvist C G Sernelius B E and Bergren K-F 1988 Optical properties of sputter- deposited ZnO: Al thin films *Thin Solid Films* 164 381-386
[28] Fan Z and Lu J G 2005 Gate-refreshable nanowire chemical sensors *Applied Physical Letters* 86 123510-123510-3
[29] Park J Y Song D E and Kim S S 2008 An approach to fabricating chemical sensors based on ZnO nanorod arrays *Nanotechnology* 19 105503-105508
[30] Huang X J and Choi Y K 2007 Chemical sensors based on nanostructured materials *Sensors and Actuators B* 122 659-671
[31] Clausen C A Green F Kartel S N 2010 Weatherability and leach resistance of wood impregnated with nano-zinc oxide *Nanoscale Res. Lett.* 5 1464-1467
[32] Zvekic D Srdic V V Karaman M A and Matavulj M N 2011 Antimicrobial properties of ZnO nanoparticles incorporated in polyurethane varnish *Processing and Application of Ceramics* 5 41-45
[33] Chithrani B D Ghazani A A and Chan W C 2006 Determining the size and shape dependence of gold nanoparticle uptake into mammalian cells *Nano. Lett.* 6 662–668
[34] Wilhelm C Gazeau F Roger J Pons J N and Bacr J C 2002 Interaction of anionic superparamagnetic nanoparticles with cells: Kinetic analyses of membrane adsorption and subsequent internalization *Langmuir* 18 8148-8155
[35] Sondi I and Salopek-Sondi B 2004 Silver nanoparticles as antimicrobial agent: a case study on< i> E. coli</i> as a model for Gram-negative bacteria *Journal of Colloid and Interface Science* 275 177-182
[36] Franklin N M Rogers N J Apte S Batley G Gadd G and Casey A 2007 Comparative toxicity of nanoparticulate ZnO, bulk ZnO, and $ZnCl_2$ to a freshwater microalga (Pseudokirchneriella subcapitata): The importance of particle solubility *Environ. Sci. Technol.* 41 8484–8490
[37] Padmavathy N Vijayaraghavan R 2008 Enhanced bioactivity of ZnO nanoparticles—an antimicrobial study *Sci. Technol. Adv. Mater.* 9 035004 (7pp).
[38] Meulenkamp E A 1998 Synthesis and growth of ZnO nanoparticles *J.Phys. Chem.* B 102 5566-5572
[39] Patterson A L 1939 The Scherrer formula for X-ray particle size determination *Physical Review* 56 978-982

[40] Mcknight D M Bencala K E Zellweger G W Alken G R Feder G L Thorn K A 1992 Sorption of dissolved organic carbon by hydrous aluminum and iron oxides occurring at the confluence of Deer Creek with the Snake River, Summit County, Colorado *Environ.Sci.Technol.* 26 1388-1396

[41] Hoyer P and Weller H 1995 Potential-dependent electron injection in nanoporous colloidal ZnO films *J.Phys. Chem.* 99 14096-14100

[42] Sluyters-Rehbach M Ijzermans A B Timmer B Griffioen and J B Sluyters J H 1966 On the impedance of galvanic cells—XVII. The mechanism of the Zn< sup> 2+</sup>/Zn (Hg) electrode reaction *Electrochimica Acta* 11 483-494

[43] Ginger D S and Greenham N C 2000 Charge injection and transport in films of CdSe nanocrystals *J. Appl. Phys.* 87 1361-1368

[44] Zhou H S Honma I and Komiyama H 1993 Coated semiconductor nanoparticles; the cadmium sulfide/lead sulfide system's synthesis and properties *J. Phys. Chem.* 97 895-901

[45] Poznyak S K Osipovich N P Shavel A Talapin D V Gao M Eychmuller A and Gaponik N 2005 Size-dependent electrochemical behavior of thiol-capped CdTe nanocrystals in aqueous solution *J. Phys. Chem. B* 109 1094-1100

[46] Grieve K Mulvaney P and Grieser F 2000 Synthesis and electronic properties of semiconductor nanoparticles/quantum dots *Current Opinion in Colloid & Interface Science* 5 168-172

[47] Li M and Li J C 2006 Size effects on the band-gap of semiconductor compounds *Materials Letters* 60 2526–2529

[48] Mudunkotuwa I A Rupasinghe T Wu C-M and Grassian V H 2012 Dissolution of ZnO nanoparticles at circumneutral pH: a study of size effects in the presence and absence of citric acid *Langmuir* 28 396-403

[49] Degen A and Kosec M 2000 Effect of pH and impurities on the surface charge of zinc oxide in aqueous solution *Journal of European Ceramic Society* 20 667-673

[50] Zhang S, Nelson A and Beales P 2012 Freezing or wrapping: The role of particle size in the mechanism of nanoparticle–biomembrane interaction *Langmuir* 28 12831–12837